Real-Time Reconstruction of Remote Sensing Imagery: Aggregation of Robust Regularization with Neural Computing

Yuriy V. Shkvarko and **Ivan E. Villalon-Turrubiates**
CINVESTAV del IPN, Unidad Guadalajara,
Av. López Mateos Sur 590, Apartado Postal 31-438, Guadalajara, C.P. 45090, JAL., MEXICO
Tel: (5233) 31345570 + 2041, Fax: (5233) 31345579 + 2329, E-mail: shkvarko@gdl.cinvestav.mx

Abstract - The robustified numerical technique for real-time sensor array reconstructive image processing is developed as required for remote sensing imaging with large scale array/synthesized array radars. The addressed technique is designed via performing the regularized robustification of the fused Bayesian-regularization imaging method aggregated with the efficient real-time numerical implementation scheme that employs the neural network computing.

Keywords: Image reconstruction, regularization, neural networks.

I. INTRODUCTION

Modern applied theory of reconstructive image processing is now a mature and well developed research field, presented and detailed in many works [AST, 97]…[WEH, 94]. Although the existing theory offers a manifold of statistical and descriptive regularization techniques for reconstructive imaging in many application areas there still remain some unresolved crucial theoretical and processing problems related to *large scale sensor array real-time reconstructive image processing*.

In this study, as a particular application area, we consider the reconstructive remote sensing (RS) imaging with the use/fusion of array sensor systems, e.g. array radars [SHK, 02], [HEN, 98] or synthetic aperture radars (SAR) [SHK, 2-04], [CUT, 90]. The particular problems that we are going to detail and treat in this paper relate to substantial reduction of the computational load of the recently developed optimal/suboptimal nonlinear Bayesian/regularization image reconstruction procedures [SHK, 1-04], [HAY, 92] via performing their robustification aggregated with efficient real-time numerical implementation that employs the neural network (NN) computing.

Two principal algorithmic-level and NN computational-level developments constitute major innovative contributions of this study, namely:

1) Development of the robustified version of the fused Bayesian-regularization (FBR) method [SHK, 1-04], [SHK, 02] for reconstruction of the power spatial spectrum pattern (SSP) of the wave field scattered from the remotely sensing scene (that is referred to as a desired RS image [FAL, 89]) given a finite set of array radar/SAR signal recordings. Since this is in essence a nonlinear numerical inverse problem, we propose to alleviate the problem ill-poseness by robustification of the Bayesian estimation strategy [FAL, 89], [HAY, 92] via performing the non adaptive approximations of the reconstructive operators that incorporate the non trivial metrics considerations for designing the proper solution space and different regularization constraints imposed on a solution. Pursuing such an approach we develop the family of robustified versions of the FBR method of different computational complexity that we address as the robustified real-time RS image reconstruction algorithms.

2) Design of numerical techniques for efficient real-time computational implementation of such robustified RS image reconstruction/enhancement algorithms that employ the NN computing. In particular, we propose to employ the general Li's architecture of the Hopfield-type dynamic NN detailed in [SHK, 01] but modify the specifications of the NN's parameters (i.e. synaptic weights and bias inputs in all the NN's loops, as well as the NN's state update rule) to enable such the modified NN to perform the real-time robust image reconstruction/enhancement tasks. Also, we propose a method to perform such a reconstruction with controllable balance between the achievable spatial resolution and admissible noise level in the resulting image.

II. PROBLEM MODEL

Consider the measurement data wavefield $u(\mathbf{y}) = s(\mathbf{y}) + n(\mathbf{y})$ modeled as a superposition of the echo signals s and additive noise n and is assumed to be available for observations and recordings within the prescribed time-space observation domain $Y \ni \mathbf{y}$, where $\mathbf{y} = (t, \mathbf{p})^{\mathrm{T}}$ defines the time-space points in the observation domain $Y = T \times P$.

The model of the observation wavefield u is specified by the linear stochastic equation of observation (EO) of operator form [SHK, 1-04]: $u = Se + n$; $e \in \mathrm{E}$; $u, n \in \mathrm{U}$; S: $\mathrm{E} \to \mathrm{U}$, on the Hilbert signal spaces E and U with the metric structures induced by the inner products, $[u_1, u_2]_{\mathrm{U}}$ and $[e_1, e_2]_{\mathrm{E}}$, respectively. The operator model of the stochastic EO in the conventional integral form may be rewritten as [FAL, 89]

$$u(\mathbf{y}) = \int_X S(\mathbf{y},\mathbf{x})\, e(\mathbf{x})\, d\mathbf{x} + n(\mathbf{y}) \ , \qquad (1)$$

$$e(\mathbf{x}) = e(f;\boldsymbol{\rho},\boldsymbol{\theta}) = \int_F e(t;\boldsymbol{\rho},\boldsymbol{\theta}) \exp(-j2\pi f t)\, dt \qquad (2)$$

where the functional kernel $S(\mathbf{y},\mathbf{x})$ of the signal formation operator (SFO) S given by (1) defines the signal wavefield formation model [WEH, 94]. Following the multi-scale array/SAR radar RS problem phenomenology [DAD, 84], [CUT, 90] we assume an incoherent nature of the backscattered field $e(\mathbf{x})$ over the frequency-space observation domain $X = F \times R = F \times P \times \Theta$, in the slant range $\boldsymbol{\rho} \in P$ and azimuth angle $\boldsymbol{\theta} \in \Theta$ domains, respectively.

When tackling the RS spatial analysis problems, the radar engineers typically work in the frequency-space domain, $\mathbf{x} = (f;\ \boldsymbol{\rho},\ \boldsymbol{\theta})^{\mathrm{T}} \in X = F \times P \times \Theta$, [SHK, 1-04], [CUT, 90], [WEH, 94]. However, because of the one-to-one mapping, only the spatial cross range coordinates $\mathbf{r} = (\boldsymbol{\rho},\ \boldsymbol{\theta})$ may be associated with $\mathbf{x}$ as well [WEH, 94]. Such interpretation is valid if one assumes the narrowband system model [HEN, 98] and incoherent nature of the backscattered field $e(\mathbf{x})$ [WEH, 94]. This is naturally inherent to the RS imaging experiments [WEH, 94], [PON, 03] in which case the phasor $e(f,\ \mathbf{r})$ in (2) is taken to be independent random variable at each frequency f, and spatial coordinates $\mathbf{r}, \boldsymbol{\theta}$ with the zero mean value and δ-form correlation function, $R_E(f,\ f';\ \mathbf{r},\ \mathbf{r}') = \langle E(f;\ \mathbf{r}) E^*(f',\ \mathbf{r}') \rangle = B(f,\ \mathbf{r}) \delta(f - f') \delta(\mathbf{r} - \mathbf{r}')$ that enables one to introduce the following definition of the spatial spectrum pattern (SSP) of the wavefield sources distributed in the observation environment [SHK, 02]

$$b(\mathbf{r}) = Aver^{(2)}\{e(\mathbf{r})\} = \int_F \langle e(f,\ \mathbf{r}) e^*(f,\ \mathbf{r}) \rangle\, |H(f)|^2\, df \ ; \quad \mathbf{r} \in R:\ \boldsymbol{\rho} \in P;\ \boldsymbol{\theta} \in \Theta. \qquad (3)$$

Here, $\langle \cdot \rangle$ represents the ensemble averaging operator, while $Aver^{(2)}$ is referred to as the second order (i.e. nonlinear) statistical averaging operator defined by (3). Also in (3), $H(f)$ represents the given transfer function of the radar receiving channels that we assume to be identical for all antenna array elements and impose the conventional normalization, $|H(f)|^2 = 1$ for all frequencies $f \in F$ in the radar receiver frequency integrating band F, [HEN, 98].

The RS imaging problem is to find an estimate $\hat{b}(\mathbf{r})$ of the SSP $b(\mathbf{r})$ in the environment $R \ni \mathbf{r}$ by processing whatever values of measurements of the data $u(\mathbf{y})$; $\mathbf{y} \in Y$, are available. For an array with arbitrary sensor configuration, the recorded data is traditionally expressed as an algebrized version of the EO (1)

$$\mathbf{U} = \mathbf{S}\mathbf{E} + \mathbf{N} \qquad (4)$$

where $\mathbf{E}$, $\mathbf{N}$ and $\mathbf{U}$ define the zero-mean vectors composed of the coefficients E_k, N_m, and U_m of the numerical approximations (decomposition [SHK, 02]) of the relevant operator-form EO (1), i.e. $\mathbf{E}$ represents the K-D vector composed with the coefficients $\{E_k = [e,\ g_k]_{\mathrm{E}},\ k = 1, \ldots, K\}$ of the K-D approximation, $e_{(K)}(\mathbf{x}) = (P_{\mathrm{E}(K)}e)(\mathbf{x}) = \sum E_k g_k(\mathbf{r})$, of the initial wavefield $e(\mathbf{x})$, and $P_{\mathrm{E}(K)}$ is a projector onto the K-D approximation subspace $\mathrm{E}_{(K)} = P_{\mathrm{E}(K)}\mathrm{E} = \mathrm{Span}\{g_k\}$ spanned by some properly chosen set of K basis functions $\{g_k(\mathbf{r})\}$ [SHK, 02], [SHK, 04]. The M-by-K matrix $\mathbf{S}$ that approximates the SFO in (4) is given now by [SHK, 02]

$$S_{mk} = [\, Sg_k, \varphi_m \,]_{\mathrm{U}} \ ;\ m = 1, \ldots, M \ ;\ k = 1, \ldots, K \qquad (5)$$

where the set of the base functions $\{\varphi_m(\mathbf{y})\}$ that span the finite-dimensional spatial observation subspace $\mathrm{U}_{(M)} = P_{\mathrm{U}(M)}\mathrm{U} = \mathrm{Span}\{\varphi_m\}$ defines the corresponding projector $P_{\mathrm{U}(M)}$ induced by these array spatial response characteristics $\{\varphi_m(\mathbf{y})\}$ [14]. Following the radar array/SAR processing terminology [FAL, 89], [CUT, 90] we refer to the kth column vector $\mathbf{s}_k$ of the SFO matrix

$$\mathbf{S} = (\mathbf{s}_1 \ \ldots\ \mathbf{s}_k \ \ldots\ \mathbf{s}_K) \qquad (6)$$

as the corresponding *array directional vector*. The vectors $\mathbf{E}$, $\mathbf{N}$ and $\mathbf{U}$ are characterized by the correlation matrices $\mathbf{R}_{\mathbf{E}} = \mathbf{D} = \mathbf{D}(\mathbf{B}) = \mathrm{diag}(\mathbf{B})$ (a diagonal matrix with vector $\mathbf{B}$ at its main diagonal), $\mathbf{R}_{\mathbf{N}}$, and $\mathbf{R}_{\mathbf{U}} = \mathbf{S}_0\mathbf{R}_{\mathrm{E}}\mathbf{S}_0^{+} + \mathbf{R}_{\mathbf{N}}$, respectively. (Recall that superscript $^{+}$ defines the adjoint operator [SHK, 1-04] that becomes the Hermitian conjugate when stands with matrix or vector). The vector, $\mathbf{B}$, is composed of the elements $B_k = \langle E_k E_k^* \rangle$; $k = 1, \ldots, K$, and is referred to as a K-D vector-form approximation of the SSP. In the array finite-dimensional formalism, the RS imaging problem is to derive an estimator for reconstructing the K-D approximation

$$\hat{b}_{(K)}(\mathbf{r}) = \left\langle \left| \hat{e}_{(K)}(\mathbf{r}) \right|^2 \right\rangle = \sum_{k=1}^{K} \hat{B}_k\, |g_k(\mathbf{r})|^2 = \mathbf{g}^{\mathrm{T}}(\mathbf{r})\, \mathrm{diag}(\hat{\mathbf{B}})\, \mathbf{g}(\mathbf{r}) ; \quad \mathbf{r} \in R \qquad (7)$$

of the SSP distribution $b(\mathbf{r})$ in the environment $R \ni \mathbf{r}$. Here $\mathbf{g}(\mathbf{r})$ denotes the vector composed of the basis functions $\{g_k(\mathbf{r})\}$ and $\hat{\mathbf{B}}$ represents the estimate of the SSP vector $\mathbf{B}$. The experiment design (ED) aspects of this problem involving the analysis of how to choose (finely adjust) the basis functions $\{g_k(\mathbf{r})\}$ that span the signal representation subspace $\mathrm{E}_{(K)} = P_{\mathrm{E}(K)}\mathrm{E} = \mathrm{Span}\{g_k\}$ for a given observation subspace $\mathrm{U}_{(M)} = \mathrm{Span}\{\varphi_m\}$ were investigated in more details in our previous studies [SHK, 02], [SHK, 1-04]. Also, we employ here the ED considerations regarding the metrics structure in the solution space defined by the inner product [SHK, 1-04]

$$\|\mathbf{B}\|^2_{B(K)} = [\mathbf{B}, \mathbf{MB}] \qquad (8)$$

where **M** is referred to as the metrics inducing operator. Hence, the selection of **M** provides the additional geometrical degrees of freedom of the problem model. In this paper, we incorporate the model of **M** that corresponds to the numerical approximation of the Tikhonov's stabilizer of the second order that was numerically designed in [SHK, 02]. Also, following [SHK, 1-04] we incorporate the projection-type a priori information requiring that the SSP vector **B** satisfies the linear constraint equation

$$\mathbf{GB} = \mathbf{C}, \text{ i.e. } \mathbf{G}^{-}\mathbf{GB} = \mathbf{B}_P \qquad (9)$$

where $\mathbf{B}_P = \mathbf{G}^{-}\mathbf{C}$ and $\mathbf{G}^{-}$ is the Moore-Penrose pseudoinverse of a given projection operator $\mathbf{G}$: $B_{(K)} \rightarrow B_{(Q)}$, and the constraint vector $\mathbf{C} \in B_{(Q)}$ and the constraint subspace $B_{(Q)}$ ($Q < K$) are assumed to be given. In (9), the constraint operator **G** projects the portion of the unknown SSP onto the subspace where the SSP values are fixed by **C**. In practice, such limitations may specify the system calibration [WEH, 94].

The main purpose of this paper is to present the efficient real-time implementation techniques for the robustified (suboptimal) versions of the fused Bayesian-regularization (FBR) optimal estimator derived previously in [SHK, 02], [SHK, 1-04] via performing the relevant array data processing. Thus we limit our study here to the implementation aspects of the SSP estimation problem via performing the robustification of the FBR method [SHK, 2-04] for the generalized model (3) of the SSP of the wavefield sources collected (integrated) over the prescribed frequency observation band. Such a generalization distinguishes the present study from the frequency independent SSP estimation that was considered in [SHK, 02], [SHK, 2-04].

III. SUMMARY OF THE FBR METHOD

The estimator that produces the optimal estimate $\hat{\mathbf{B}}$ of the SSP vector via processing the M-D data recordings **U** applying the FBR estimation strategy that incorporates nontrivial a priori geometrical and projection-type model information was developed in our previous study [SHK, 1-04]. Such optimal FBR estimate of the SSP is given by the nonlinear equation [SHK, 04] that we generalize here for the case of the integrated SSP model as follows,

$$\hat{\mathbf{B}} = \mathbf{B}_P + \mathbf{PB}_0 + \mathbf{W}(\hat{\mathbf{B}})\{\mathbf{V}(\hat{\mathbf{B}}) - \mathbf{Z}(\hat{\mathbf{B}})\}. \qquad (10)$$

In (10), $\mathbf{B}_P$ is defined by (9) and $\mathbf{B}_0$ represents the a priori SSP distribution to be considered as a zero step approximation to the desires SSP $\hat{\mathbf{B}}$. Note that in this paper, we use all the notations from [SHK, 1-04] for definitions of the sufficient statistics (SS) vector $\mathbf{V}(\hat{\mathbf{B}}) = \{\mathbf{F}(\hat{\mathbf{B}})\mathbf{U}\mathbf{U}^{+}\mathbf{F}^{+}(\hat{\mathbf{B}})\}_{\text{diag}}$ ($\{\cdot\}_{\text{diag}}$ determines a vector composed of the principal diagonal of the embraced matrix), the solution-dependent SS formation operator

$$\mathbf{F} = \mathbf{F}(\hat{\mathbf{B}}) = \mathbf{D}(\hat{\mathbf{B}})(\mathbf{I} + \mathbf{S}^{+}\mathbf{R}_{\mathbf{N}}^{-1}\mathbf{SD}(\hat{\mathbf{B}}))^{-1}\mathbf{S}^{+}\mathbf{R}_{\mathbf{N}}^{-1}; \qquad (11)$$

the SS shift vector $\mathbf{Z}(\hat{\mathbf{B}})$ [SHK, 1-04], and the composite solution-dependent smoothing-projection window operator [SHK, 2-04]

$$\mathbf{W}(\hat{\mathbf{B}}) = \mathbf{P}\boldsymbol{\Omega}(\hat{\mathbf{B}}) \qquad (12)$$

with the projector

$$\mathbf{P} = (\mathbf{I} - \mathbf{G}^{-}\mathbf{G}) \qquad (13)$$

and the solution-dependent smoothing window

$$\boldsymbol{\Omega}(\hat{\mathbf{B}}) = (\text{diag}\{\{\mathbf{S}^{+}\mathbf{F}^{+}\mathbf{FS}\}_{\text{diag}}\} + \hat{\alpha}\,\mathbf{D}^2(\hat{\mathbf{B}})\mathbf{M}(\hat{\mathbf{B}}))^{-1} \qquad (14)$$

in which the regularization parameter $\hat{\alpha}$ is to be adaptively adjusted using the system calibration data [SHK, 2-04].

As it was analyzed in [SHK, 2-04], because of the complexity of the solution dependent K-D operator inversions needed to be performed to compute the SS $\mathbf{V}(\hat{\mathbf{B}})$, the window $\mathbf{W}(\hat{\mathbf{B}})$ and SS shift $\mathbf{Z}(\hat{\mathbf{B}})$, the computational load of the original optimal FBR estimator (10) is *extremely high* to address that as a practically realizable estimator of the SSP (i.e. practical high-resolution RS radar imaging technique realizable in a real-time mode).

IV. ROBUSTIFIED FBR TECHNIQUES

A. FBR-Robustified Estimator

In this subsection, we propose the robustification scheme for real-time implementation of the FBR estimator (10) that enables one to reduce drastically the computation load of the image formation procedure without substantial degradation in the resolution and overall image performances. We propose the robustified version of the FBR estimator (referred to as R-FBR method) via roughing $\mathbf{P} = \mathbf{I}$ and performing the robustification (nonadaptive approximation) of both the SS formation operator $\mathbf{F}(\hat{\mathbf{B}})$ and the smoothing window $\boldsymbol{\Omega}(\hat{\mathbf{B}})$ in (10) by roughing $\mathbf{D}(\hat{\mathbf{B}}) \approx \mathbf{D} = \beta\mathbf{I}$, where β represents the expected a priori image gray level [SHK, 02]. Hence, the robustified SS formation operator

$$\mathbf{F} = \mathbf{A}^{-1}(\rho)\mathbf{S}^{+} \quad \text{with} \quad \mathbf{A}(\rho) = \mathbf{S}^{+}\mathbf{S} + \rho^{-1}\mathbf{I} \qquad (15)$$

becomes the regularized inverse of the SFO **S** with regularization parameter ρ^{-1}, the inverse of the signal-to-noise ratio (SNR) $\rho = \beta/N_0$ for the adopted white noise model, $\mathbf{R}_{\mathbf{N}} = N_0\mathbf{I}$. The robust smoothing window

$$\mathbf{W} = \boldsymbol{\Omega} = (w_0\mathbf{I} + \mathbf{M})^{-1} \qquad (16)$$

is completely defined now by the matrix **M** that induces the metrics structure (8) in the solution space [PON, 03] with the scaling factor $w_0 = \mathrm{tr}\{\mathbf{S}^+\mathbf{F}^+\mathbf{F}\mathbf{S}\}/K$. Note that such robustified **W** can be pre-computed a priori for a family of different admissible ρ as it was performed in the previous study [SHK, 02]. Here, we adopt practical constraints of high SNR operational conditions [STA, 98], [GAL, 04] ρ >> 1, in which case one can neglect also the constant bias $\mathbf{Z} = Z_0\mathbf{I}$ in (10) because it does not affect the pattern of the SSP estimate (it influences only the constant gray level in the resulting solution but $Z_0 << \beta$ for ρ >> 1). Following these practically motivated assumptions, the resulting R-FBR estimator becomes

$$\hat{\mathbf{B}}_{RFBR} = \mathbf{B}_0 + \mathbf{\Omega}\mathbf{V} \qquad (17)$$

where $\mathbf{V} = \{\mathbf{F}\mathbf{U}\mathbf{U}^+\mathbf{F}^+\}_{\mathrm{diag}}$ represents now the robust (solution independent) SS vector. Thus, the principal computational load of the R-FBR estimator (17) is associated now with the operator inversions required to compute the solution operator (15) for adaptively (recurrently) adjusted regularization parameter ρ.

B. Matched Spatial Filtering Estimator

The simplest rough SSP estimator can be constructed as further simplification of (17) if we adopt the trivial a priori model information ($\mathbf{P} = \mathbf{I}$ and $\mathbf{B}_0 = 0\mathbf{I}$) and roughly approximate the SS formation operator **F** by the adjoint SFO, i.e. $\mathbf{F} \approx \gamma_0\mathbf{S}^+$ [SHK, 2-04] (where the normalizing constant γ_0 provides balance of the operator norms $\gamma_0^2 = \mathrm{tr}^{-1}\{\mathbf{S}^+\mathbf{S}\mathbf{S}^+\mathbf{S}\}\mathrm{tr}\{\mathbf{F}\mathbf{S}\mathbf{S}^+\mathbf{F}^+\}$). In that case, the estimator (17) is simplified to its rough version

$$\hat{\mathbf{B}}_{MSF} = \mathbf{\Omega}\,\mathbf{H} \qquad (18)$$

where the rough SS $\mathbf{H} = \gamma_0^2\{\mathbf{S}^+\mathbf{U}\mathbf{U}^+\mathbf{S}\}_{\mathrm{diag}}$ is now formed applying the adjoint operator $\mathbf{S}^+$, and the windowing of the rough SS **H** is performed applying the smoothing filter $\mathbf{\Omega} = (w_0\mathbf{I} + \mathbf{M})^{-1}$ with the nonnegative entry, the same one as was constructed numerically in [SHK, 02]. The (18) can be referred to as *matched estimator* of the SSP. This definition will become apparent from the following explanation.

C. Remark 1

Observe, that (18) is recognized to be a vector-form representation of the conventional kernel SSP estimation algorithm [SHK, 04], in which the SS is formed as the squared modulus of the outcomes of the matched spatial filter applied to the recorded data signal (trajectory signal in the SAR terminology [SHK, 2-04], [CUT, 90]). Thus, in the framework of the FBR inference-based approach to RS imaging [SHK, 1-04], the traditional matched filtering technique (18) can be viewed as a rough simplified version of the developed above R-FBR method. In view of this, in the presented family of the SSP estimators, we specify (18) as the rough matched spatial filtering (MSF) method for SSP estimation, whereas we refer to (17) as the robustified FBR (R-FBR) enhanced RS imaging method and (10) as the complete FBR-optimal SSP reconstruction technique, respectively.

V. NN FOR IMPLEMENTING THE R-FBR METHOD

In this Section, we propose the NN for efficient real-time computational implementation of the above presented R-FBR method. The main idea is to aggregate the robust regularization with the NN-based computing to reduce the computational load of the R-FBR method. We approach this goal by performing the modifications of the multistate Hopfield-type modified NN originally developed in [SHK, 01]. The modification that we perform is aimed at enabling such the NN to implement computationally the R-FBR algorithm (17). Borrowing from [SHK, 01] we define the Hopfield-type NN as a massive interconnection of formal neurons, i.e. basic processing units. The outputs of all *K* neurons compose the output vector, $\mathbf{z} = \mathrm{sgn}(\mathbf{Q}\mathbf{v} + \mathbf{\Theta})$, where, **Q** represents the $K \times K$ matrix of the interconnection strengths of the NN, and **Θ** defines the $K \times 1$ bias vector of the NN [SHK, 01]. The output vector **z** is used to update the state vector **v** of the network: $\mathbf{v}'' = \mathbf{v}' + \Delta\mathbf{v}$ where, $\Delta\mathbf{v} = \Re(\mathbf{z})$ is a change of the state vector **v** computed applying the state update rule $\Re(\mathbf{z})$ [SHK, 01] and the superscripts ″ and ′ correspond to the state values before and after network state updating, respectively. The state update rule $\Re(\mathbf{z})$ is designed in such a way [SHK, 01] that the energy function of the overall NN

$$E_{NN}(\mathbf{v}) = -\frac{1}{2}\mathbf{v}^{\mathrm{T}}\mathbf{Q}\mathbf{v} - \mathbf{\Theta}^{\mathrm{T}}\mathbf{v} \qquad (19)$$

is decreased at each updating step, i.e. $E_{NN}(\mathbf{v}'') \le E_{NN}(\mathbf{v}')$, until the NN reaches its stationary state (saddle point) related to the state $\mathbf{v}_{opt}$ at which the minimum of the NN energy (19) is attained, i.e. $E_{NN}(\mathbf{v}_{opt}) = \min_{v} E_{NN}(\mathbf{v})$. Analyzing now the behavior of such the NN we may associate the NN's stationary state with the solution to the hypothetical inverse problem (*IP*) of minimization of the composite cost function

$$E_{IP}(\mathbf{Y}|\boldsymbol{\lambda}) = \frac{1}{2}\lambda_1\|\mathbf{U} - \mathbf{S}\mathbf{Y}\|^2 + \frac{1}{2}\lambda_2\|\mathbf{Y}\|^2. \qquad (20)$$

If the regularization parameters in (20) are adjusted as $\lambda_1 = 1$, $\lambda_2 = \rho^{-1}$ and the NN's stationary state is associated with the solution to (20) than minimization of $E_{IP}(\mathbf{Y}|\boldsymbol{\lambda})$ provides the robust constraint least square (CLS) estimate $\mathbf{Y} = \mathbf{F}\mathbf{U}$ that uniquely defines the desired high-resolution SSP vector $\mathbf{V} = \{\mathbf{Y}\mathbf{Y}^+\}_{\mathrm{diag}}$. Hence, the cumbersome operator inversions needed to compute the SS formation operator (15) can be translated into the

relevant problem of recurrent minimization of the energy function (19) of the NN and derivation of $\mathbf{Y} = \mathbf{v}_{opt}$ via specification of the NN's parameters as follows**:**

$$Q_{ki} = -\lambda_1 \sum_{j=1}^{K} S_{jk} S^*_{ji} - \lambda_2 \delta_{ki} \quad ; \qquad (21)$$
$$\text{for all } k, I = 1, \ldots, K.$$

$$\Theta_k = \lambda_1 \sum_{j=1}^{K} S_{jk} U_j \quad ; \qquad (22)$$
$$\text{for all } k = 1, \ldots, K.$$

where Q_{ki} and Θ_k represent the elements of the interconnection strengths matrix **Q** and bias vector **Θ** of the modified NN, respectively.

A. Remark 2

Observe that because of the exclusion of the solution-dependent operator inversions (15) via translations (21), (22) of the SS formation procedure into the relevant recurrent problem of minimization of the NN's energy function (19) associated with the relevant $E_{IP}(\mathbf{Y}|\boldsymbol{\lambda})$ (20) the computational load of the R-FBR procedure (17) is drastically decreased in comparison with the fully optimal FBR algorithm (10).

In the simulation applications (reported in the subsequent Section) related to the 512×512 pixel image format, the computation load of the RS enhanced imaging with the R-FBR algorithm (17) applying the proposed above NN computational scheme in comparison with the original FBR method (10) was decreased approximately 10^5 times and required 0.38 sec of the overall computational time (i.e. real-time mode) for implementing the R-FBR technique (17) with the SONY VGN-A190 PC.

VI. SIMULATIONS

In the simulations, we assumed the SAR with partially/fractionally synthesized array as an RS imaging system [SHK, 2-04]. The SFO was factorized along two axes in the image plane: the azimuth (horizontal axis) and the range (vertical axis).

Following the common practically motivated technical considerations [WEH, 94] we modeled a triangular shape of the SAR range ambiguity function of 3 pixels width, and a |*sinc*| shape of the side-looking radar antenna radiation pattern of 10 pixels width at the zero crossing level for the first scenario of fractionally synthesized array (System 1), and 20 pixels width for the second scenario of fractionally synthesized array (System 2), respectively.

We examined the behavior and performance indices of the derived above estimators for different simulated scenes of the SSPs and two RS system configurations.

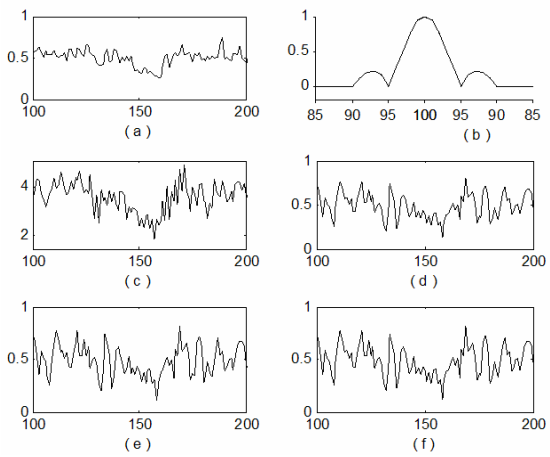

Fig. 1. Simulation results for 1-*D* scenario: 1st system model. (a) Original scene. (b) Point Spread Function. (c) Noised MSF image. (d) CLS reconstructed image. (e) FBR reconstructed image. (f) R-FBR reconstructed image.

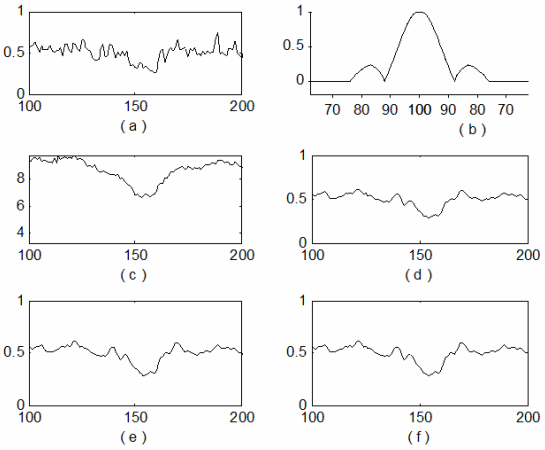

Fig. 2. Simulation results for 1-*D* scenario: 2nd system model. (a) Original scene. (b) Point Spread Function. (c) Noised MSF image. (d) CLS reconstructed image. (e) FBR reconstructed image. (f) R-FBR reconstructed image.

The 1-*D* simulated SSP (for one particular SAR range gate) is presented in Fig. 1.a. The other pictures of Fig. 1 report the formed/reconstructed images obtained with the 1st simulated system configuration applying three different estimators as specified in the figure captions.

The 1-*D* simulated SSP (for the same particular SAR range gate) is presented in Fig. 2.a. The other pictures of Fig. 2 report the formed/reconstructed images obtained with the 2nd simulated system applying three different estimators as specified in the figure captions.

Figures 3.a and 4.a show the 2-*D* 512-by-512 pixel format scene images originally formed via implementing the MSF method with the RS imaging system data provided by the simulated RS imaging Systems of model 1 and model 2, respectively.

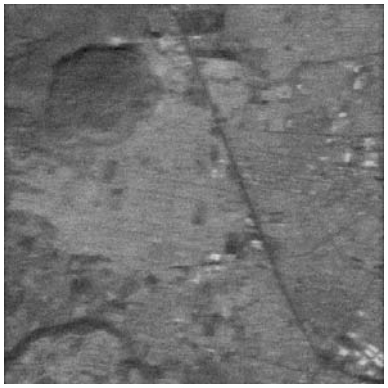

(a)

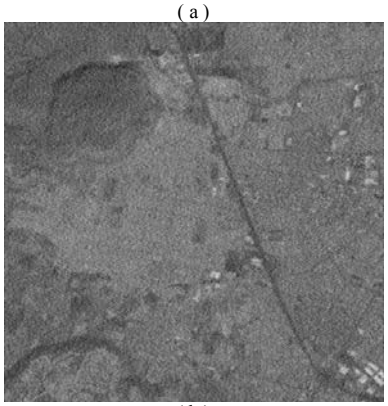

(b)

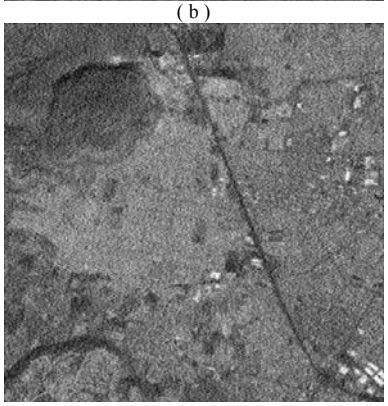

(c)

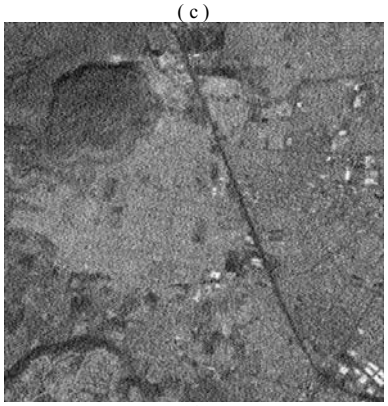

(d)

Fig. 3. Simulation results for System 1: (a) Noised MSF image. (b) CLS reconstructed image. (c) FBR reconstructed image. (d) R-FBR reconstructed image.

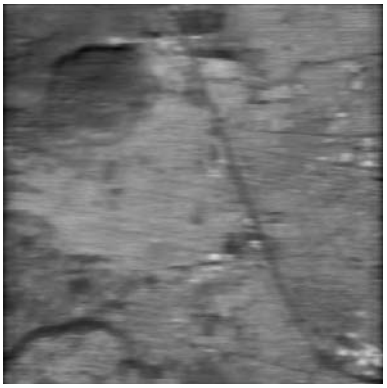

(a)

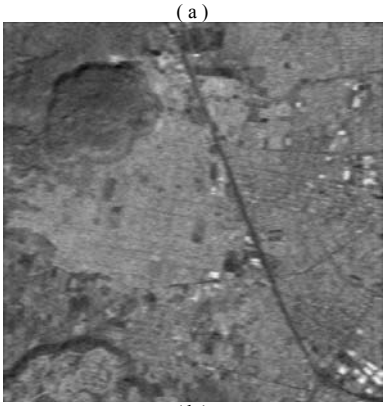

(b)

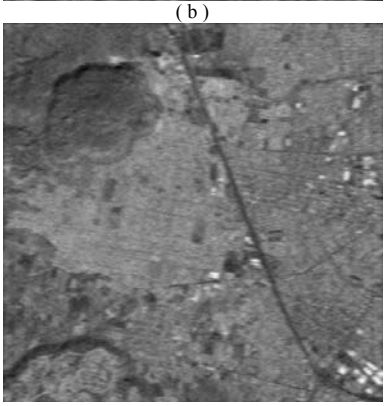

(c)

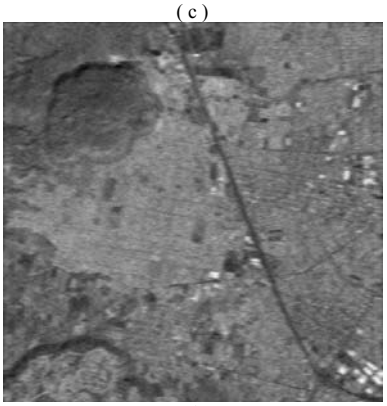

(d)

Fig. 4. Simulation results for System 2: (a) Noised MSF image. (b) CLS reconstructed image. (c) FBR reconstructed image. (d) R-FBR reconstructed image.

Table 1. IOSNR values provided with the two simulated methods. Results are reported for different simulated SNRs for two different system models.

SNR	System 1			System 2		
(dB)	CLS	R-FBR	FBR	CLS	R-FBR	FBR
10	2.35	2.42	2.56	19.49	20.26	21.12
15	5.15	5.56	5.78	20.42	21.83	22.97
20	8.24	8.72	8.95	21.25	22.66	23.85
25	12.71	13.19	14.34	21.13	22.54	23.71
30	17.54	17.91	18.12	22.18	23.59	24.60

Figures 3.b and 4.b present the reconstructed (enhanced) images formed using the *CLS* algorithm for System 1 and System 2, respectively. Figures 3.c and 4.c present the images reconstructed applying the *FBR* algorithm for System 1 and System 2, respectively. Figures 3.d and 4.d present the images reconstructed applying the *R-FBR* algorithm for System 1 and System 2, respectively.

These examples of 2-D simulations of two RS imaging systems are presented for the same fractional aperture synthesis scenarios as in the 1-D cases, respectively. The quantitative measure of the improvement in the output signal-to-noise ration (*IOSNR*) [SHK, 02] gained with the enhanced imaging methods for the two simulated fractional aperture synthesis scenarios are reported in Table I.

VII. CONCLUDING REMARKS

We have developed and presented the R-FBR method for real-time high resolution SSP estimation as required for reconstructive RS imagery although it may also be applied to other fields. The developed R-FBR method was implemented in real-time mode utilizing the proposed Hopfield-type multi-state NN computational technique.

The interconnection strengths and bias inputs of the designed NN were specified in such a way that enabled the NN to perform solution of the aggregate inverse problem of high-resolution SS estimation (i.e. RS image reconstruction) from the available array data recordings required to implement the overall R-FBR method. The developed technique performs the balanced aggregation of the data and model information to perform the efficient image reconstruction with improved spatial resolution and noise reduction in real-time mode.

The presented simulation examples illustrate the overall imaging performance improvement gained with the proposed approach. The presented study establishes the foundation to assist in understanding the basic theoretical aspects of the multi-level suboptimal RS image processing that aggregates the robust regularization and NN-computing paradigms with controllable reduction of the computational load of the image reconstruction tasks as required for particular applications related to large scale array/SAR RS imagery, although, the results can be extended to other practical areas in real-time imaging systems design and applications.

REFERENCES

[AST, 97] J. Astola and P. Kuosmanen, Fundamentals of Nonlinear Digital Filtering. Boca Raton, FL: CRC, 1997.

[CUT, 90] L.G. Cutrona, "Synthetic Aperture Radar," in *Radar Handbook*, 2nd ed., M.I. Skolnik, Ed. in chief, MA: McGraw Hill, 1990.

[DAD, 84] E. Dadgeon, and R.M. Merserau, Multidimensional Digital Signal Processing. Englewood Cliffs, NJ: Prentice Hall, 1984.

[FAL, 89] S.E. Falkovich, V.I. Ponomaryov, and Y.V. Shkvarko, Optimal Reception of Space-Time Signals in Channels With Scattering (in Russian). Moscow: Radio i Sviaz, 1989.

[GAL, 04] Gallegos-Funes F.J. and Ponomaryov V.I., "Real-Time Image Filtering Scheme Based on Robust Estimators in Presence of Impulsive Noise", *Real Time Imaging VII*, Elsevier Publ., pp. 69-80, 2004.

[HAY, 92] S. Haykin and A. Steinhardt, Eds., Adaptive Radar Detection and Estimation. New York: Wiley, 1992.

[HEN, 98] F.M. Henderson and A. V. Lewis, Eds., Principles and Applications of Imaging Radar, Manual of Remote Sensing, 3rd ed. New York: Willey, 1998, vol. 3.

[PON, 03] Ponomaryov V.I. and Nino-de-Rivera L., "Order statistics – M Method in Image and Video Sequence Processing Applications", Electromagnetic Waves and Electronic Systems, Moscow: ISSN 1560-4128, Vol. 8, N7-8, pp. 99-107, 2003.

[PUE, 96] R.C. Puetter, "Information, language, and pixon-based image reconstruction", *Proc. SPIE*, vol. 2827, pp. 12-31, 1996.

[SHK, 01] Y.V. Shkvarko, Y.S. Shmaliy, R. Jaime-Rivas, and M. Torres-Cisneros, "System fusion in passive sensing using a modified Hopfield network", Journal of the Franklin Institute, vol. 338, pp. 405-427, June 2001.

[SHK, 02] Y.V. Shkvarko, "Estimation of wavefield power distribution in the remotely sensed environment: Bayesian maximum entropy approach," IEEE Trans. Signal Proc., vol. 50, pp. 2333-2346, Sep. 2002.

[SHK, 1-04] Y.V. Shkvarko, "Unifying regularization and Bayesian estimation methods for enhanced imaging with remotely sensed data. Part I – Theory", IEEE Trans. Geoscience and Remote Sensing, vol. 42, pp. 923-931, March 2004.

[SHK, 2-04] Y.V. Shkvarko, "Unifying regularization and Bayesian estimation methods for enhanced imaging with remotely sensed data. Part II – Implementation and performance issues", IEEE Trans. Geoscience and Remote Sensing, vol. 42, pp. 932-940 , March 2004.

[STA, 98] J.L. Starck, F. Murtagh, and A. Bijaoui, Image Processing and Data Analysis. The Multiscale Approach, Cambridge, U.K.: Cambridge Univ. Press, 1998.

[WEH, 94] D.R. Wehner, High-Resolution Radar, 2-nd ed. Boston: Artech House, 1994.